REPORT DOCUMENTATION PAGE

Form Approved OMB NO. 0704-0188

1. REPORT DATE (DD-MM-YYYY)	2. REPORT TYPE	3. DATES COVERED (From - To)
25-07-2012	Conference Proceeding	-

4. TITLE AND SUBTITLE
Evaluation and Improvement of Spectral Features for the Detection of Buried Explosive Hazards Using Forward-Looking Ground-Penetrating Radar

5a. CONTRACT NUMBER
W911NF-08-1-0188

5b. GRANT NUMBER

5c. PROGRAM ELEMENT NUMBER
633606
654808

6. AUTHORS
Justin Farrell, Timothy C. Havens, Dominic K. C. Ho, James M. Keller, Tuan T. Ton, David C. Wong, Mehrdad Soumekh

5d. PROJECT NUMBER

5e. TASK NUMBER

5f. WORK UNIT NUMBER

7. PERFORMING ORGANIZATION NAMES AND ADDRESSES
University of Missouri - Columbia
Office of Sponsored Programs
The Curators of the University of Missouri
Columbia, MO 65211 -

8. PERFORMING ORGANIZATION REPORT NUMBER

9. SPONSORING/MONITORING AGENCY NAME(S) AND ADDRESS(ES)
U.S. Army Research Office
P.O. Box 12211
Research Triangle Park, NC 27709-2211

10. SPONSOR/MONITOR'S ACRONYM(S)
ARO

11. SPONSOR/MONITOR'S REPORT NUMBER(S)
54379-CS.21

12. DISTRIBUTION AVAILIBILITY STATEMENT
Approved for public release; distribution is unlimited.

13. SUPPLEMENTARY NOTES
The views, opinions and/or findings contained in this report are those of the author(s) and should not contrued as an official Department of the Army position, policy or decision, unless so designated by other documentation.

14. ABSTRACT
We provide an evaluation of spectral features extracted from the signal return of a forward-looking ground penetrating radar to improve the detection performance of buried explosive hazards. The evaluations are performed on data collected at two different lanes at a government test site. The performance of the one-dimensional (1D), two-dimensional (2D) and multiple (ML) spectral features will be contrasted through lane-based cross-validation for training and testing. Additional features to characterize the spectral behaviors of the forward-looking radar

15. SUBJECT TERMS
forward looking ground penetrating radar, explosive hazards, detection, signal processing, spectral features

16. SECURITY CLASSIFICATION OF:			17. LIMITATION OF ABSTRACT	15. NUMBER OF PAGES	19a. NAME OF RESPONSIBLE PERSON
a. REPORT	b. ABSTRACT	c. THIS PAGE			Dominic Ho
UU	UU	UU	UU		19b. TELEPHONE NUMBER: 573-882-8023

Report Title

Evaluation and Improvement of Spectral Features for the Detection of Buried Explosive Hazards Using Forward-Looking Ground-Penetrating Radar

ABSTRACT

We provide an evaluation of spectral features extracted from the signal return of a forward-looking ground penetrating radar to improve the detection performance of buried explosive hazards. The evaluations are performed on data collected at two different lanes at a government test site. The performance of the one-dimensional (1D), two-dimensional (2D) and multiple (ML) spectral features will be contrasted through lane-based cross-validation for training and testing. Additional features to characterize the spectral behaviors of the forward-looking radar return will also be examined.

Conference Name: Conf. Detection and Sensing of Mines, Explosive Objects, and Obscured Targets XVII

Conference Date: July 23, 2012

Evaluation and Improvement of Spectral Features for the Detection of Buried Explosive Hazards Using Forward-Looking Ground-Penetrating Radar

Justin Farrell[a], Timothy C. Havens[a], K.C. Ho[a], James M. Keller[a],
Tuan T. Ton[b], David C. Wong[b], and Mehrdad Soumekh[c]
[a]Dept. of Electrical and Computer Engineering, University of Missouri, Columbia, MO, USA 65211;
[b]U.S. Army RDECOM CERDEC Night Vision & Electronic Sensors Directorate,
Fort Belvoir, Virginia, USA 22060;
[c]Dept. of Electrical Engineering, University of New York at Buffalo, Amherst, NY, USA 14260

ABSTRACT

We provide an evaluation of spectral features extracted from the signal return of a forward-looking ground penetrating radar to improve the detection performance of buried explosive hazards. The evaluations are performed on data collected at two different lanes at a government test site. The performance of the *one-dimensional* (1D), *two-dimensional* (2D) and *multiple* (ML) spectral features will be contrasted through lane-based cross-validation for training and testing. Additional features to characterize the spectral behaviors of the forward-looking radar return will also be examined.

Keywords: forward looking ground penetrating radar, explosive hazards, detection, signal processing, spectral features

1. INTRODUCTION

Forward looking ground penetrating radar (FLGPR) is a viable technology for the detection of buried explosives that enables comfortable standoff distance. The detection task, however, is very challenging because of the low radar signal return strength, the lack of depth information, and the inadequate spatial resolution.

Previous attempts for target detection using FLGPR have been focusing on the intensity map generated from the beam-formed radar return image.[1-7] When exploiting the fact that a higher intensity could indicate signal reflection from a buried target, a simple detector based on size-contrast processing has been developed.[8] The detector provides a reasonable detection performance. The amount of false alarms, however, is high since any reflections from the ground, such as a piece of wood or a rock, can induce detections.

To reduce the amount of false alarms, frequency domain approaches have been explored.[9-11] The frequency domain approach looks into the spatial variation of the FLGPR return in the cross-track dimension to reduce the number of false detections. The spatial variation is assessed through the *Fast Fourier Transform* (FFT) of the FLGPR data over a short cross-track segment centered at an alarm location. The FFT magnitudes at several frequency bins are collected to form the 1D spectral features. The previous work has shown that 1D spectral features are very effective in reducing the numbers of false detections caused by clutter objects.[11]

The robustness of the 1D spectral features can be improved by using multiple 1D spectral features at several down-track positions located ahead and beyond an alarm location. This is because the declared alarm location may often be a few scans off from the actual target location. We shall denote the multiple 1D spectral features as ML spectral features.

Both the 1D and ML spectral features capture the variations of the FLGPR signal return in the cross-track dimension only and variations from the down-track dimension are ignored. It is logical to extend the ML approach by using a square spatial window centered at an alarm declaration and apply 2-dimensional FFT to obtain better spectral features. We call this approach the 2D spectral feature.

In our previous work, the 1D, ML and 2D spectral features were introduced.[11] However, because of the lack of data, no cross-validation results were presented for comparisons. This paper provides a more vigorous performance evaluation using data from multiple runs along two different lanes at a government test site. Our results show that the performances

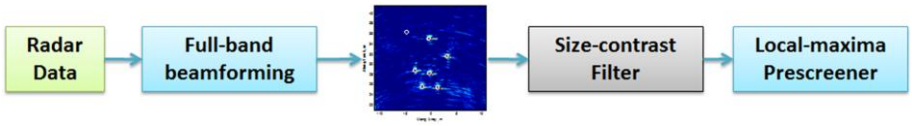

(a) FLGPR beamforming and prescreeener

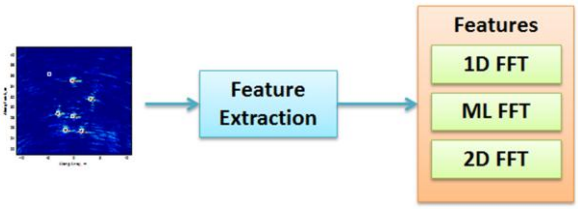

(b) Spectral feature extraction

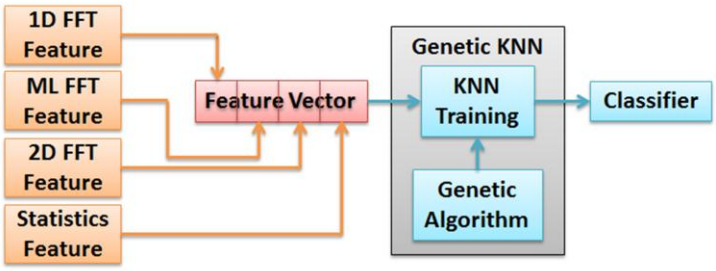

(c) Genetic KNN classifier

Figure 1. FLGPR explosive hazard detection block diagram

of the three spectral features are comparable, with 2D giving slightly better results, followed by ML and 1D. The spectral features are found to reduce the amount of false alarms for the size-contrast based detector.

Figure 1 illustrates our explosive hazard detection approach. In view (a), we show that the radar data is beamformed, then size-contrast filtered, and a candidate set of alarm locations is determined using a local-maxima prescreener. View (b) illustrates the feature extraction. For each alarm, 3 features are extracted: 1D, ML, and 2D FFT-based features. Finally, these features are used to train a KNN classifier, which classifies incoming alarms as false alarm or true-positive.

We shall summarize briefly in Section 2 the computation of the 1D, 2D and ML spectral features. A few statistical features will be introduced to better measure the frequency domain characteristics of the FLGPR signal return. Section 3 provides the description of the data used for evaluation. Section 4 is the experimental results, shown as *receiver operating characteristic* (ROC) curves, and Section 5 is the conclusion.

1.1 ALARIC FLGPR

The FLGPR images we use in this paper were collected using a system called ALARIC. This system is an FLGPR that is composed of a physical array of sixteen receivers and one transmitter. The T/R array is aimed about 8 meters in front of the vehicle with approximately a 35 degree grazing angle relative to the ground. In the past decade, FLGPR systems have primarily used their physical arrays (aperture) as well as their radar bandwidth for achieving high resolution imaging; conventional backprojection or time-domain correlation imaging has been used for this purpose. Those systems rarely tried to exploit imaging information that is created by the motion of the platform. The ground-based FLGPR community has referred to imaging methods that leverage platform motion as multi-look imaging. Though, in the airborne community, this is better known as *synthetic aperture radar* (SAR) imaging. SAR has been shown to be an effective tool for airborne *intelligence*, *surveillance* and *reconnaissance* (ISR) applications.

Table 1. ALARIC FLGPR Image-Forming Parameters

Parameter	*Value*
Coherent integration range	5 – 10 meters down-range
Full-band bandwidth	100 MHz – 1.5 GHz
Down-range image resolution	5 cm
Cross-range image resolution	3 cm
Cross-range detection limits	-5 to +5 meters

The ALARIC system is equipped with an accurate GPS system. As a result, it is capable of processing both physical and synthetic aperture imaging, even when the platform moves along a nonlinear or curved path. To create the FLGPR images, a nonlinear processing technique called *Adaptive Multi-Transceiver Imaging* is used. This method exploits a measure of similarity among the 32 T/R images which adaptively suppresses artifacts such as sidelobes and aliasing ghosts.

Table 1 contains the parameters of the ALARIC FLGPR that were used to create the images used in this paper. The FLGPR images are created for an area -11 to +11 meters in the cross-range direction—although only the -5 to +5 meter cross-range sub-region is used in our detection algorithms—where negative numbers indicate to the left of the vehicle. Coherent integration of the radar scans is done in a 5 meter area, starting 5 meters in front of the vehicle. The pixel-resolution of the FLGPR image is 5 cm in the down-range and 3 cm in the cross-range directions. The center frequency is 800 MHz and the bandwidth is 1.4 GHz. The detection region we use is 10 meters wide, centered in the cross-range direction.

1.2 Miss-distance halo size

In this paper, we present results for a 1 meter radius miss-distance halo. There are many mechanisms of error in FLGPR that do not exist in downward-looking sensors, such as refraction at the air-ground boundary and other soil boundary layers, longer range imaging (which accentuates geo-location-based errors), and low-grazing angle specular ground-bounce. As of yet, a comprehensive understanding of how these sources of error manifest into miss-distances does not exist. Furthermore, we believe that FLGPR can operate as an early-warning sensor, cueing operators to the presence of targets ahead. The operators can then slow down and use a downward-looking system to more accurately locate the hazard. This allows operators to overall travel at higher speeds, covering more terrain in less time. Next we describe the prescreener.

1.3 Prescreener

Consider an FLGPR image $I(u,v)$ where u is the cross-range coordinate and v is the down-range coordinate. This image is first size-contrast filtered and then input to a local-maxima finding algorithm to determine candidate alarm locations. Our prescreener first calculates the size-contrast filtered image $I_{sc}(u,v)$. This image is then used to find local maxima, which we identify as candidate target locations. A size-contrast filter is a simple operation defined by

$$I_{sc}(u,v) = \min\{I_{center}(u,v) - I_{halo}(u,v), 0\}, \tag{1}$$

where $I_{center}(u,v)$ is the mean pixel value in the center of a surrounding halo of pixels and $I_{halo}(u,v)$ is the mean pixel value within the surrounding halo region. The center value $I_{center}(u,v)$ is calculated as

$$I_{center}(u,v) = \frac{1}{(2x+1)(2y+1)} \sum_{\substack{i=-x:x \\ j=-y:y}} I(u-i, v-j), \tag{2}$$

where *x* and *y* determine the size of the box in which the pixels are added. The halo value $I_{halo}(u,v)$ is computed by

$$I_{halo}(u,v) = \frac{1}{(2x_h+1)(2y_h+1) - (2x+1)(2y+1)} \left[\sum_{\substack{i=-x_h:x_h \\ j=-y_h:y_h}} I(u-i, v-j) - \sum_{\substack{i=-x:x \\ j=-y:y}} I(u-i, v-j) \right] \tag{3}$$

It is easy to see that the images $I_{center}(u,v)$ and $I_{halo}(u,v)$, for all u, v in the image, can be computed by convolution. The image $I_{center}(u,v)$ is calculated by convolving $I(u,v)$ with a rectangle of size $(2x+1, 2y+1)$, each pixel having a value of the preceding fraction in (2). Similarly, $I_{halo}(u,v)$ is calculated by convolving $I(u,v)$ with a halo with inner

dimensions $(2x+1,2y+1)$ and outer dimensions $(2x_h+1,2y_h+1)$; each pixel in the halo has a value of $1/[(2x_h+1)(2y_h+1)-(2x+1)(2y+1)]$. We empirically tested many values of the size-contrast parameters and found that (x,y,x_h,y_h) worked the best in general (although, the results for similarly sized and shaped filters were virtually identical). These are the parameter values we use for the results presented in this paper.

After $I_{sc}(u,v)$ is calculated, we pass this image through a local-maxima finding algorithm. Our method first computes a maximum order-filtered image with a 3 meter x 1 meter rectangular kernel. We denote this order-filtered image as $O_{sc}(u,v)$. Essentially, each pixel in the size-contrast filtered image is replaced by the maximum pixel value within a 3 meter cross-range and 1 meter down-range rectangle, centered on the pixel. Figure 2 shows an example of an FLGPR image in view (a), its respective size-contrast filtered image in view (b), and its associated order-filtered image in view (c). As this figure shows, the order-filter reduces the effect that noise-induced artifacts have on finding "hot spots" in the image. Alarms are identified by the operation

$$A = \arg_{(u,v)}\{I_{sc}(u,v) \geq \min\{O_{sc}(u,v), 10\}\},$$

where A is the set of local-maxima locations. The minimum operator prescreens alarm locations that have a very low image value (confidence). We chose a value of 10 for this threshold as this only eliminates alarms with the lowest of confidences. This prescreening threshold merely minimizes the computational cost of the subsequent algorithms by reducing the number of alarms to a manageable number. We also annotate the alarm locations A with the value of the size-contrast image pixel at each location, which we denote as $I_{sc}(A)$. This pixel value is, in effect, the confidence of the alarm—the higher the value, the higher the confidence. Figure 2 illustrates the prescreener process, including the alarm locations for the example images shown. The next step is to calculate a set of feature vectors for each alarm in A.

2. SPECTRAL FEATURES

These features capture the spatial spectrum of the alarm locations. In previous works, we found that true positive alarm locations exhibited different spectral characteristics than FAs. Here we present three types of spectral features, each of which is extracted from each alarm location in A.

The second and fourth rows in the second column of Fig. 3 are the spectral responses of a target and a FA respectively. As this figure illustrates, there tends to be more high spatial frequency content in a FA than with a target. There are three different forms of spectral features explored in this work, a 1D FFT in the cross track direction, multiple 1D cross track

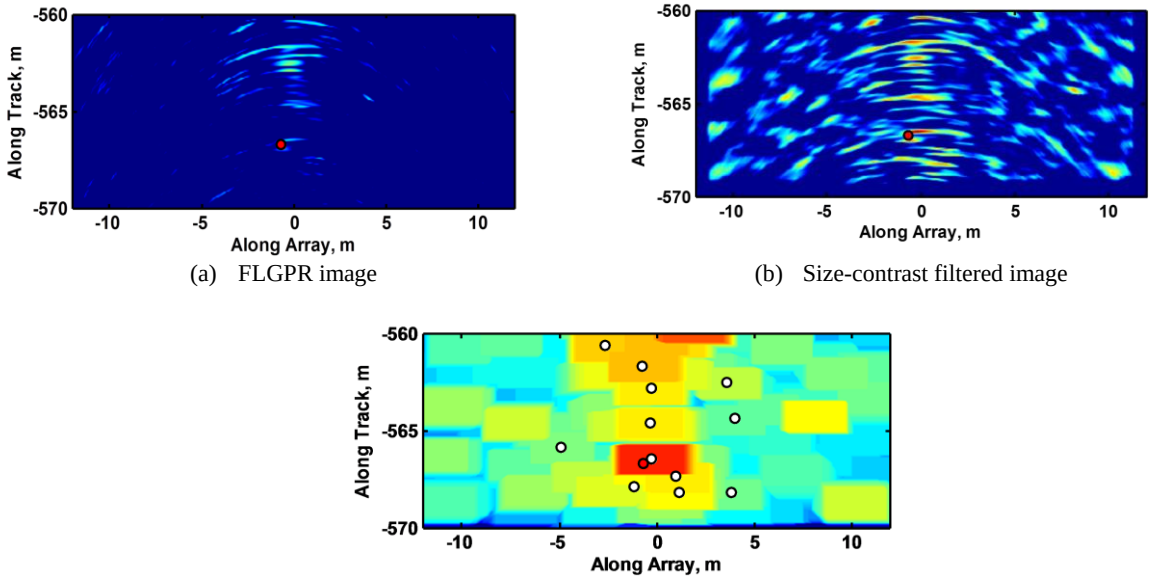

(a) FLGPR image

(b) Size-contrast filtered image

(c) Local-maxima detector image

Figure 2. Prescreener images—Target shown by red circle, alarm locations shown by white circles

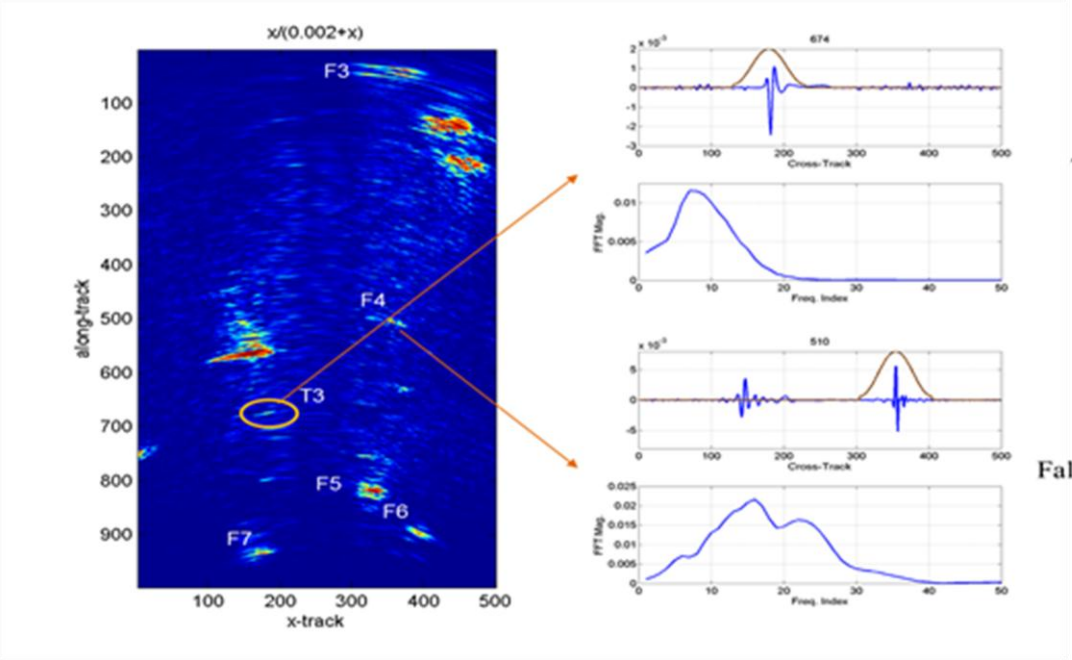

Figure 3. Illustration of spectral features in the cross track direction and the difference between actual targets and FAs.

FFTs in the down track direction, and a 2-dimensional FFT.

To further improve detection performance, features are extracted that can be used to delineate a positive detection and *false alarm* (FA) classes. It is important to find features that have separation between these two classes in the feature space. As previously shown, spectral characteristics of background clutter differ from those of explosive hazards. This difference is exploited to train a classifier which can be used to classify incoming data as FA or true positive. Figure 3 highlights the difference between the spectral responses of a target and a FA.

2.1 1D FFT Feature in the Cross Track Direction

The radar data contain complex images from which we use only the real portion in the spectral feature extraction. At each alarm location provided by the prescreener, a 1D FFT in the cross track direction is calculated. This is accomplished by taking a 101 point horizontal slice of pixels centered on the alarm. Then, a 101 point Hamming window is applied to this vector so that more importance is given to the center pixels of the alarm. The FFT is then performed on the row vector. The spectral features are obtained by computing the magnitudes of each frequency bin. A mathematical description of the process is

$$X_f(A) = |FFT(\mathrm{Re}[H \circ I_{101}(A)])|,$$

where $\circ$ indicates an element by element multiplication, Re indicates that the real part of the complex signal is used, H is the Hamming window, $I_{101}(A)$ is the 101-length row vector of FLGPR image pixels surrounding alarm A. We then store the first 50 frequency values (excluding the DC value) of $X_f(A)$. These 50 frequency values are the features used by the classifier. Figure 3 illustrates the output of the 1D FFT.

2.2 Multiple 1D FFT Cross Track Direction Features

The ML feature is composed of multiple 1D FFT slices. The FFT is calculated on multiple cross track slices of the radar image in the down track direction. Because the alarms are larger than one horizontal slice, using multiple slices will encompass more of the alarm and the surrounding area. This provides a more complete representation of the alarm compared to using a single slice of the image.

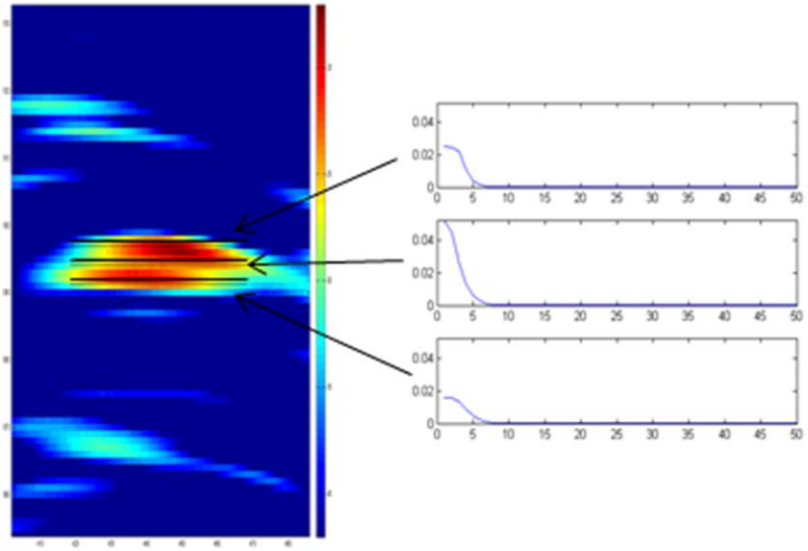

Figure 4. Illustration of the ML feature. Three cross track, from the eleven, 1D FFT features are shown.

Eleven rows of 101 pixels, five beyond the alarm, five before and one centered on the alarm, are used in the calculation of the spectral features. Again a 101 point Hamming window is used on each of the slices and a 1D FFT is calculated for each of the eleven vectors. Note that the row centered on the alarm is exactly the 1D feature. Figure 4 illustrates this concept.

Figure 4 shows three rows of the ML feature, one centered on the target, one above center, and one below center. As with the 1D case, only the magnitude's of the first 50 frequency bins are used from each FFT, which are then concatenated to produce a feature vector with 550 elements.

2.3 2D FFT Feature

Although the ML FFT captures more of the target signature, it does not contain any down-track (vertical/columns) spatial frequency information. The 2D FFT contains both cross-track and down-track information, which provides a more complete spectral description of each alarm. Although the 2D and ML FFT use more of the image to extract features and would be expected to outperform the 1D FFT, our results show that these two feature sets complement the 1D FFT very well.

To implement the 2D FFT, an image block, 101 pixels wide and 21 pixels high centered on the alarm location, is extracted. A 2D Hamming window of the same size is applied to the image block to emphasize the center of the alarm location. Then the magnitude of the 2D FFT is computed, resulting in a spectral image that is 101 (columns) x 21 (rows). The equation is

$$X_f(A) = \left| FFT_{2D}\left(\mathrm{Re}\left[H \circ I_{101,21}(A)\right]\right)\right|,$$

where $\circ$ indicates an element by element multiplication, H is a 2D Hamming window, and $I_{101,21}(A)$ is the (101 x 21) rectangular sub-image centered at A. We only use the first quadrant (the positive frequencies in both directions) of the 2D FFT, producing a spectral image block that is 50 (columns) x 10 (rows). Figure 5 shows the 2D FFT of an alarm.

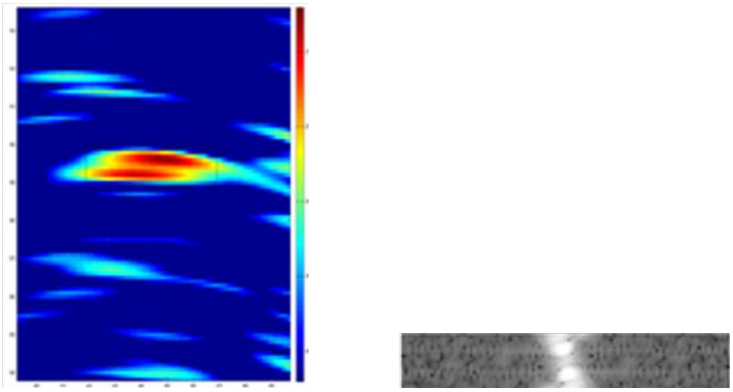

(a) FLGPR image (b) 2D FFT image

Figure 5. 2D FFT illustration

Table 1. Details of the Data Collections

	Lane-A	**Lane-B**
Total Number of Runs	5	4
Number of Eastbound Runs	2	2
Number of Westbound Runs	3	2
Date for Data Collection	5/10/2011, 5/12/2011	5/11/2011, 5/12/2011

Table 2. Distributions of the targets at different depths in the two lanes and their metal content

	Lane A		**Lane B**	
	High Metal	**Low Metal**	**High Metal**	**Low Metal**
Depth	**# of Targets**	**# of Targets**	**# of Targets**	**# of Targets**
1”	10	11	10	12
2”	3	3	4	4
3	1	4	2	4
5”	2	3	2	4
6”	3	4	4	4
Shallow: 1”-3”	14	18	16	20
Deep: 5”-6”	5	7	6	8
Total	19	25	22	28

3. DATA DESCRIPTION

The data we use here was collected over three consecutive days in May, 2011 from a U.S. government built FLGPR system. The collections were done on two lanes; lane A and lane B. There are 9 runs in the dataset, 5 from lane A and 4 from lane B. Table 1 gives the details of the data collection runs.

All of the targets in the two lanes are buried in the center of the road at various depths ranging from 1 to 6 inches. The targets consist of landmines and other explosive objects, each with different amounts of metal content. Table 2 details the target counts with respect to depths and metal content.

Lane A has 44 targets and lane B has 50. About 72% of the targets for each lane are buried at a shallow depth (1”-3”) and 44% of those shallow-buried targets have high metal content. Nearly 42% of the deeply-buried targets are high metal. Overall, about 44% of the targets have high metal content.

4. EXPERIMENTAL RESULTS

Table 4 gives the detection performance of the prescreener. The perforamance is separated for high metal and low metal targets, and for shallow (1”-3”) and deep (5”-6”) targets. The detection of metal targets is over 90%. For low-metal targets, we have about 70% detection if the target depth is shallow but only 62% when it is deep. Overall, the detection rate is 95.91% for metal targets and 68.22% for low-metal targets.

Table 4. Detection performance of the size-contrast based prescreener

	Shallow (1”-3”)	Deep (5”-6”)
Metal Targets	119 / 169 (70.41%)	42 / 69 (62.69%)
Low-Metal Targets	129 / 133 (96.99%)	41 / 45 (91.11%)

The 1D, 2D, and ML spectral features are generated at each alarm location for target/non-target classification. The classifier used is a *genetic k-nearest neighbor* (GKNN).[11] The GKNN algorithm is a standard KNN algorithm that uses a genetic algorithm to adjust the *k* parameter (the number of datums that are considered) and to perform feature selection. Lane-based cross-validations are used for training and testing. The GKNN uses cross-validation methods to maximize the *area under the ROC* (AUR) for the training data. The AUR metric is simply the normalized integrated area under the ROC curve.

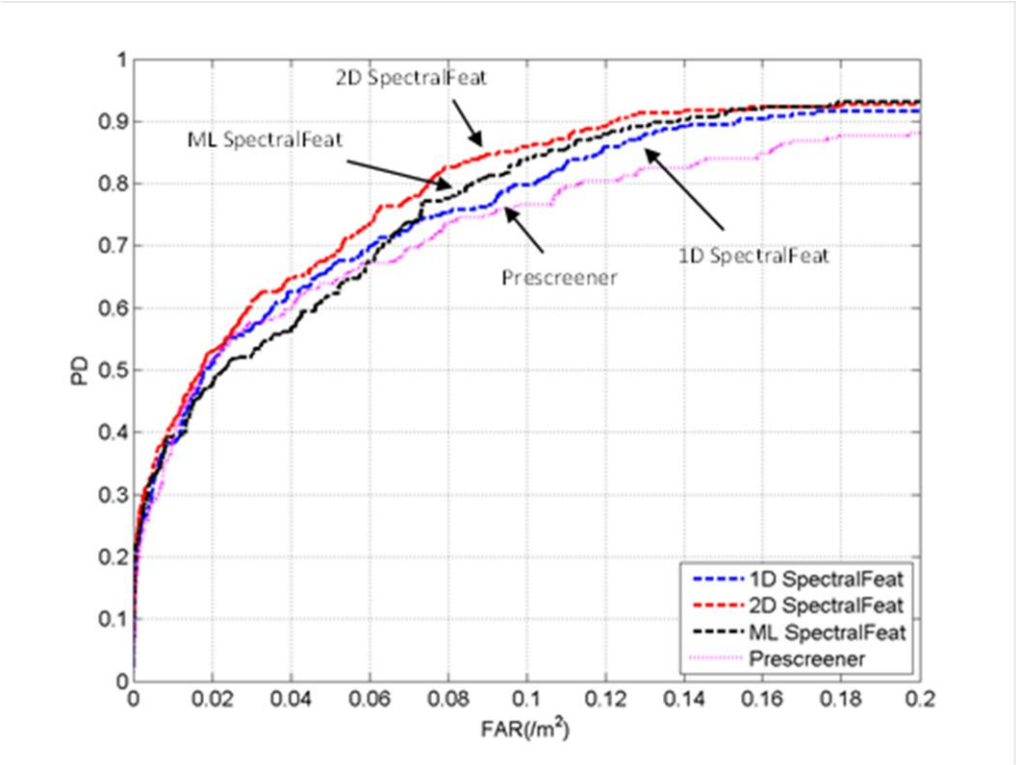

Figure 6 Comparison of 1D, 2D and ML spectral features; train on Lane A and test on Lane B

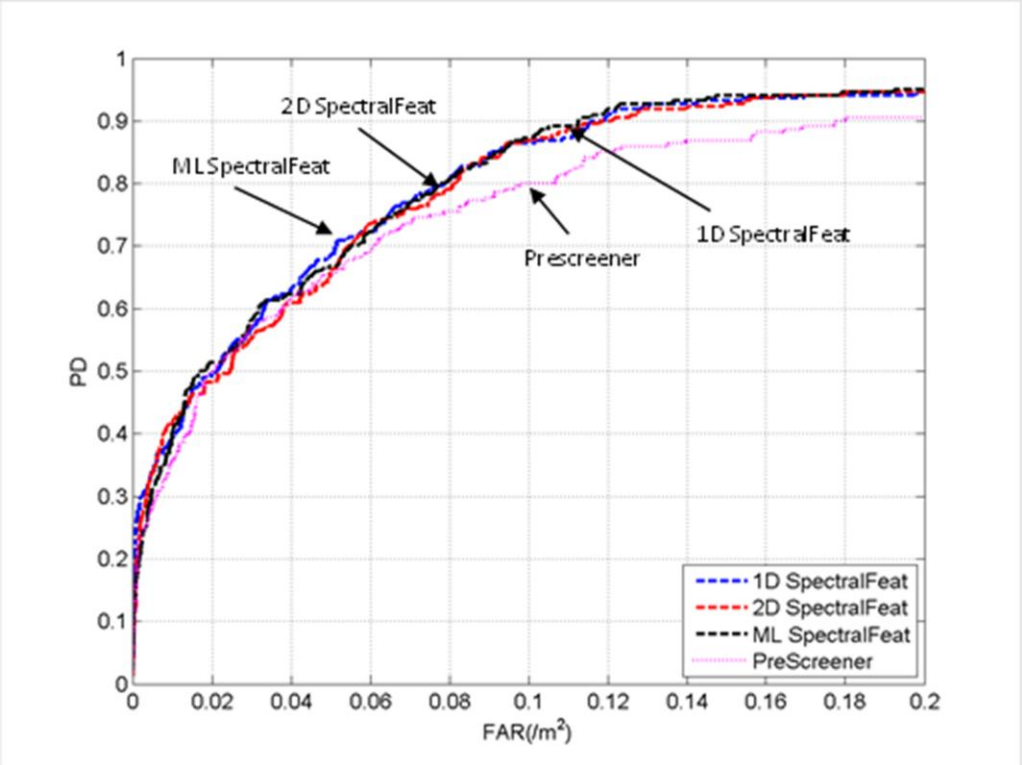

Figure 7 Comparison of 1D, 2D, and ML spectral features; train on Lane B and test on Lane A

Figure 6 gives the ROC curves when we use Lane A for training and Lane B for testing. For *probability of detection* (PD) above 70%, the 2D spectral features perform best, followed by the ML and 1D spectral features. They all provide much better performance than the prescreener. At 80% PD, the 2D spectral features achieve 55% reduction in the FAR, relative to the prescreener.

Figure 7 depicts the ROC curves when Lane B is used for training and Lane A for testing. In this case, the performances for all three spectral features are nearly identical. The performance improvement relative to the prescreener is less than the previous case. Nevertheless, the reduction in FAR is about 20% at 80% PD.

We next examine the use of statistical features computed on the frequency spectrum in addition to the spectral features to improve the detection performance. The statistical features used are the mean, standard deviation, skewness, and kurtosis of the pixels surrounding the alarm location. Only the results with 1D spectral features together with the statistical features are presented for ease of illustration.

Figure 8 shows the results when we train on Lane A and test on Lane B. Four ROC curves are presented. The four curves are the prescreener, 1D spectral features only (without using the statistical features), 1D spectral features with skewness and kurtosis, and 1D spectral features with skewness, kurtosis, mean and standard deviation. The use of skewness and kurtosis is very effective to increase the performance. Adding the mean and standard deviation features improves the results further. At 80% PD, the reduction in FAR when using the four statistical features is about 25%.

The results for training on Lane B and testing on Lane A are given in Fig. 9. The statistical features do not show much improvement. Importantly though, they do not degrade the performance.

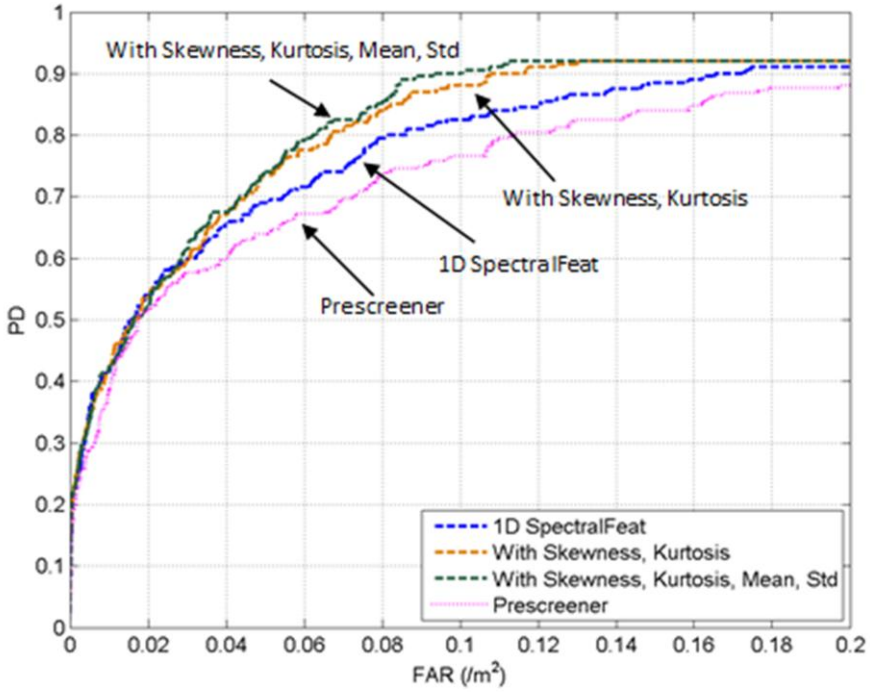

Figure 8 Performance improvement with the addition of statistical features, train on Lane-A and test on Lane-B

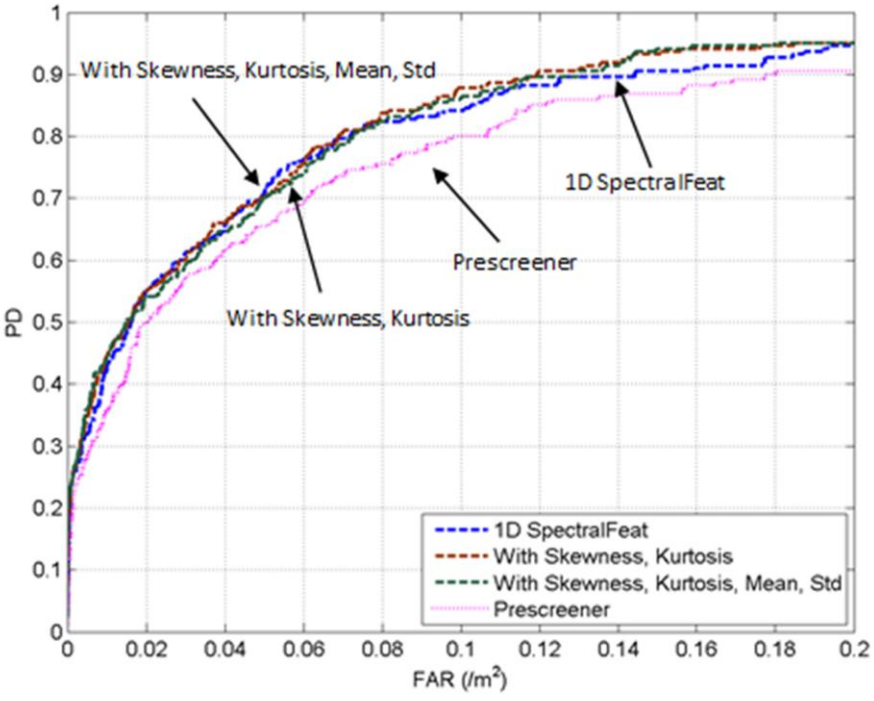

Figure 9 Performance improvement with the addition of statistical features, train on Lane B and test on Lane A

5. CONCLUSION

We have investigated and compared the performance of several variants of the spectral features using FLGPR data collected at a government test site. The 2D spectral feature provided better performance than the 1D and ML spectral features. We conjecture that this is because the 2D feature captures both the horizontal and vertical spatial variations, as opposed to the 1D and ML features, which only capture the horizontal variations. Several statistical features computed from the FLGPR frequency spectrum are also introduced. These statistical features were found to be effective in improving the performance in one lane and not in the other. Further investigations will be conducted as more data become available.

5.1 Future work

In the future, we will combine these features with our other work, which use visibile- and infrared-spectrum cameras to detect explosive hazards.[12] Furthermore, our most recent work has focused on using multiple kernel learning to fuse cell-structure features, such as local binary patterns and histograms of oriented gradients.[13] We aim to use the spectral features as an additional set of features in our multiple kernel learning approach. It is our conjecture that fusing multiple sensor modalities is an essential element of an effective explosive hazard detection system.

ACKNOWLEDGEMENTS

This work was funded by Army Research Office grant number 57940-EV to support the US Army RDECOM CERDEC NVESD and by Leonard Wood Institute grant LWI 101-022

REFERENCES

[1] Bradley, M.R., Witten, T.R., Duncan, M., and McCummins, R., "Anti-tank and side-attack mine detection with a forward-looking GPR", Proc. SPIE 5415, 421-432 (2004).
[2] Stone, K., Keller, J.M., Ho, K.C., and Gader, P.D. "On the registration of FLGPR and IR data for the forward-looking landmine detection system and its use in eliminating FLGPR false alarms," Proc. SPIE 6953, (2008).
[3] Havens, T.C., Stone, K., Keller, J.M., and Ho, K.C. "Sensor-fused detection of explosive hazards", Proc. SPIE 7303, 73032A (2009).
[4] Havens, T.C., Spain, C.J., Ho, K.C., Keller, J.M., Ton, T.T., Wong, D.C., and Soumekh, M., "Improved Detection and False Alarm Rejection Using FLGPR and Color Imagery in a Forward-Looking System", Proc. SPIE, 7664, 76641U (2010).
[5] Havens, T.C., Ho, K.C., Farrell, J., Keller, J.M., Popescu, M., Ton, T.T., Wong, D.C., Soumekh, M., "Locally adaptive detection algorithm for forward-looking ground-penetrating radar", Proc. SPIE, 7664, 76642E (2010).
[6] Wang, T., Sjahpetura, O., Keller, J.M., and Gader, P.D., "Landmine detection using forward-looking GPR with object-tracking," Proc. SPIE 5794, 1080-1088 (2005).
[7] Havens, T.C., Keller, J.M., Ho, K.C., Ton. T.T., Wong, D.C., and Soumekh, M., "Narrow-band processing and fusion approach for explosive hazard detection in FLGPR," Proc. SPIE, 8017, 80171F (2011).
[8] Gader, P.D., Grandhi, R., Lee, W.H., Wilson, J.N., and Ho, K.C., "Feature analysis for the NIITEK ground penetrating radar using order weighted averaging operators for landmine detection", Proc. SPIE 5415, 953-962 (2004).
[9] Sun, Y., and Li, J., "Plastic landmine detection using time-frequency analysis for forward-looking ground-penetrating radar", Proc. SPIE 5089, 851-862 (2003).
[10] Havens, T.C., Ho, K. C., Keller, J. M., Popescu, M., Ton, T. T., Wong, D. C. and Soumekh, M., "Locally adaptive detection algorithm for forward-looking ground-penetrating radar," Proc. SPIE 7664, 76642E (2010).
[11] Farrell, J. W., Havens, T. C., Ho, K. C., Keller, J. M., Ton, T. T., Wong, D.C. and Soumekh, M., "Detection of explosive hazards using spectrum features from forward-looking ground-penetrating radar imagery," Proc. SPIE 8017, 80171E (2011).
[12] Anderson, D.T., Keller, J.M., and Sjahputera, O., "Algorithm fusion in forward-looking longwave infrared imagery for buried explosive hazard detection," Proc. SPIE, 8017, 801722 (2011).
[13] Havens, T.C., Stone, K., Anderson, D.T., Keller, J.M., Ho, K C., Ton, T.T., Wong, D.C. and Soumekh, M., "Multiple kernel learning for explosive hazard detection in forward-looking ground-penetrating radar," to appear, Proc. SPIE (2012).